Projected Changes in Future Extreme Precipitation over the Northeast United States in the NA-CORDEX Ensemble

ROBERT H. NAZARIAN,[a] JAMES V. VIZZARD,[a] CARISSA P. AGOSTINO,[a] AND NICHOLAS J. LUTSKO[b]

[a] *Department of Physics, Fairfield University, Fairfield, Connecticut*
[b] *Scripps Institution of Oceanography, University of California, San Diego, La Jolla, California*

(Manuscript received 19 January 2022, in final form 12 September 2022)

ABSTRACT: The northeastern United States (NEUS) is a densely populated region with a number of major cities along the climatological storm track. Despite its economic and social importance, as well as the area's vulnerability to flooding, there is significant uncertainty around future trends in extreme precipitation over the region. Here, we undertake a regional study of the projected changes in extreme precipitation over the NEUS through the end of the twenty-first century using an ensemble of high-resolution, dynamically downscaled simulations from the North American Coordinated Regional Climate Downscaling Experiment (NA-CORDEX) project. We find that extreme precipitation increases throughout the region, with the largest changes in coastal regions and smaller changes inland. These increases are seen throughout the year, although the smallest changes in extreme precipitation are seen in the summer, in contrast to earlier studies. The frequency of heavy precipitation also increases such that there are relatively fewer days with moderate precipitation and relatively more days with either no or strong precipitation. Averaged over the region, extreme precipitation increases by +3%–5% $°C^{-1}$ of local warming, with the largest fractional increases in southern and inland regions and occurring during the winter and spring seasons. This is lower than the +7% $°C^{-1}$ rate expected from thermodynamic considerations alone and suggests that dynamical changes damp the increases in extreme precipitation. These changes are qualitatively robust across ensemble members, although there is notable intermodel spread associated with models' climate sensitivity and with changes in mean precipitation. Together, the NA-CORDEX simulations suggest that this densely populated region may require significant adaptation strategies to cope with the increase in extreme precipitation expected at the end of the next century.

SIGNIFICANCE STATEMENT: Observations show that the northeastern United States has already experienced increases in extreme precipitation, and prior modeling studies suggest that this trend is expected to continue through the end of the century. Using high-resolution climate model simulations, we find that coastal regions will experience large increases in extreme precipitation (+6.0–7.5 mm day^{-1}), although there is significant intermodel spread in the trends' spatial distribution and in their seasonality. Regionally averaged, extreme precipitation will increase at a rate of ~2% $decade^{-1}$. Our results also suggest that the frequency of extreme precipitation will increase, with the strongest storms doubling in frequency per degree of warming. These results, taken with earlier studies, provide guidance to aid in resiliency preparation and planning by regional stakeholders.

KEYWORDS: North America; Extreme events; Precipitation; Hydrometeorology; Regional models

1. Introduction

Changes in extreme precipitation have the potential to be among the most damaging impacts of global warming, with significant ramifications for agriculture (Rosenzweig et al. 2002), severe flooding (Tabari 2020), and landslides (Kirschbaum et al. 2012), among many other things. Observations show that global-mean extreme precipitation has increased in intensity and frequency throughout the globe over the past century (Groisman et al. 2005; Alexander et al. 2006) and numerous modeling studies suggest extreme precipitation will continue to change as the climate warms (Kao and Ganguly 2011; Fischer et al. 2013; Kharin et al. 2013; Fischer et al. 2014; O'Gorman 2015; Bao et al. 2017). The magnitude of this change, however, is regionally and model dependent. Understanding the extent to which extreme precipitation will change through the end of the century is vitally important as communities look to develop resilience to extreme precipitation and associated flooding events (Wilhelmi and Morss 2013; Gandini et al. 2020).

In the present study, we focus on extreme precipitation trends in the northeastern United States (NEUS). This region is of particular interest due to its high population density, coupled with the distribution of large cities along the climatological storm tracks (Kocin and Uccellini 2004; Zarzycki 2018). Observational studies have shown that extreme precipitation over the NEUS has increased by approximately 2%–4% $decade^{-1}$ over the past century, depending on the observational product and on the mode of analysis (Kunkel et al. 2013; Agel et al. 2015; Frei et al. 2015; Ivancic and Shaw 2016; Hoerling et al. 2016; Huang et al. 2017; Agel et al. 2018; Huang et al. 2018; Howarth et al. 2019;

Denotes content that is immediately available upon publication as open access.

Corresponding author: Robert H. Nazarian, rnazarian@fairfield.edu

DOI: 10.1175/JAMC-D-22-0008.1

Lopez-Cantu et al. 2020). These trends show substantial seasonality, with the largest increases in the warm season (i.e., June, July, August, and September) (Frei et al. 2015).

Several modeling studies have provided comparisons with observations and diagnosed potential mechanisms for the increases in precipitation (Hoerling et al. 2016; Agel et al. 2020; Agel and Barlow 2020; Huang et al. 2021). These simulations have shown relatively good agreement with observations of extreme precipitation in terms of magnitude and seasonality and have also found that resolution is of first-order importance for accurately capturing the spatial distribution of extreme precipitation. Interestingly, there is little difference in the performance of the CMIP5 and CMIP6 ensembles in the region (Agel et al. 2020; Agel and Barlow 2020), suggesting that improvements to model physics have not resulted in improved representations of the NEUS climate.

Modeling studies of future extreme precipitation over the NEUS are more limited. Sheffield et al. (2013) and Sillmann et al. (2013) evaluated CMIP5 output at the regional scale and found that, while there is some agreement in the sign of the trend in extreme precipitation over the NEUS, the magnitude differs notably between models. Furthermore, the simulated precipitation was shown to be biased low due to the coarse resolution of the models. Thibeault and Seth (2014) analyzed the CMIP5 ensemble and found that the projected increases in total annual precipitation are driven by increases in winter extreme precipitation, in contrast with the observations of Frei et al. (2015). Additionally, Thibeault and Seth (2014) found that the largest changes are projected in coastal and northern portions of the NEUS.

Hayhoe et al. (2008) and Rawlins et al. (2012) used regional climate models (RCMs) to analyze future mean and extreme precipitation in the NEUS, with both studies reporting the largest increase in winter months, as well as a coastal enhancement of precipitation. However, Hayhoe et al. (2008) analyzed monthly averaged data, which is too low resolution to use for adaptation and planning purposes, and only three models were considered, with a relatively narrow range in climate sensitivities. Similarly, the results of Rawlins et al. (2012) were presented as seasonal values, and only extended to the mid-twenty-first century. Ning et al. (2015) and Wang et al. (2020) used two independent, statistically downscaled ensembles to study extreme precipitation over the region and found consistent spatial patterns of change but very different magnitudes, as well as differences in the frequency of extreme precipitation. Ashfaq et al. (2016) and Rastogi et al. (2020) used an ensemble of CMIP5 simulations downscaled over the United States and showed that the number of extreme precipitation days that the NEUS experiences are expected to increase by midcentury.

Given the relatively limited number of modeling studies of future NEUS extreme precipitation trends, as well as the importance of resolution for accurately simulating precipitation in the region, there is an urgent need for studies of future trends in NEUS extreme precipitation using high-resolution climate model simulations. More generally, several recent studies have shown that dynamically downscaled GCM simulations using high-resolution RCMs can provide "added value" in capturing smaller-scaled climate processes relative to using only GCMs (Diffenbaugh et al. 2005; Di Luca et al. 2012; Ashfaq et al. 2016; Lucas-Picher et al. 2017), as RCMs capture a greater number of the mesoscale phenomena that lead to extreme precipitation. RCMs also afford more realistic representations of surface forcing (such as orography) (Leung et al. 2003) and of the atmosphere's circulation, both of which contribute to more realistic projections of extreme precipitation [although the convective parameterizations in both GCMs and RCMs have been shown to inadequately capture convectively driven extreme precipitation (O'Gorman 2015; Muller and Takayabu 2020)].

With this motivation, in the present study we examine projected trends in extreme precipitation over the NEUS in the Coordinated Regional Climate Downscaling Experiment (CORDEX). CORDEX consists of dynamically downscaled GCM simulations, designed using the CMIP5 GCM ensemble, and serves to evaluate and improve regional climate downscaling models and techniques, as well as to explore regional climate processes. To study trends in extreme precipitation in the NEUS, we use the North American CORDEX (NA-CORDEX) ensemble, which provides downscaled simulations over the North American region. The ensemble members in NA-CORDEX sample nearly the entire range of climate sensitivity in CMIP5 (Bukovsky and Mearns 2020), and thus can be expected to provide a realistic representation of model uncertainty in future warming. In contrast, the ensembles of driving GCMs used in prior studies of future trends over the NEUS had significantly narrower ranges of climate sensitivity. Furthermore, NA-CORDEX uses the CMIP5 ensemble, whereas previous studies, such as Rawlins et al. (2012), were based on an older generation of models used in the North American Regional Climate Change Assessment Program. The mean state of the NA-CORDEX simulations has been previously analyzed by Lucas-Picher et al. (2017), Karmalkar (2018), and Bukovsky and Mearns (2020), and uncertainty in extreme precipitation over the NA-CORDEX domain was briefly discussed by Lopez-Cantu et al. (2020) in a larger study of extreme precipitation projections over the continental United States. A detailed analysis of trends in both annual and seasonal extreme precipitation over the NEUS in the NA-CORDEX suite of simulations has not yet been conducted.

Our analysis includes regional-average trends in extreme precipitation as well as local trends, and we examine both annual-mean and seasonal changes—in winter, extreme precipitation over the NEUS is associated with large-scale frontal systems or extratropical cyclones, whereas, in summer, extreme precipitation tends to occur in isolated convective systems or in tropical cyclones. We also investigate the potential drivers of extreme precipitation changes over the NEUS in terms of thermodynamic and dynamic contributions. While increases in extreme precipitation are expected due to warmer air's ability to hold more water vapor, dynamical changes can modify this picture. We also examine the intermodel spread in extreme precipitation changes across the NA-CORDEX ensemble members for both the annual and seasonal analyses. Throughout the analysis, we relate our results to both prior regional

studies of the NEUS as well as to global studies of midlatitude precipitation.

The remainder of the paper is organized as follows. In section 2, we describe the NA-CORDEX data, the metrics by which we define extreme precipitation, and the techniques used in the analysis. In section 3 we present the main results, and in section 4 we offer further synthesis of the pertinent results, avenues for future research, and conclusions.

2. Materials and methods

a. *Models and simulations*

At the time of writing, the only available version of NA-CORDEX is based on the CMIP5 suite of simulations (Bukovsky and Mearns 2020; McGinnis and Mearns 2021); a revised CORDEX program using CMIP6 is in its early stages of development and the downscaled simulations have not yet been conducted. However, as mentioned in section 1, Agel and Barlow (2020) found that there was little improvement in the simulation of extreme precipitation over the NEUS in the CMIP6 suite of simulations relative to the CMIP5 suite of simulations [despite the different forcing scenarios of CMIP5 (RCPs) and CMIP6 Shared Socioeconomic Pathways (SSPs)] and so, assuming the revised CORDEX will use the same RCMs (at the time of writing this has not yet been decided), we expect that our findings will be qualitatively robust in the next generation of experiments.

NA-CORDEX simulations are publicly available at 0.44°, 0.22°, and 0.11° resolution. We use the simulations with 0.22° (25 km) resolution, since the smaller subset of simulations available at 0.11° resolution only cover the historical period. Even if 0.11° simulations were available for future emission scenarios, we expect that they would be largely consistent with the 0.22° simulations, as Lucas-Picher et al. (2017) found that historical 0.22° and 0.11° simulations showed good agreement over the NEUS, and both provided improved agreement with observations relative to 0.44°-resolution simulations using a variety of metrics. These improvements were attributed, in part, to better representation of orography.

We use model data that were previously interpolated onto a common grid to provide straightforward comparisons between models (McGinnis and Mearns 2021). While data are available for the entire continental United States, we only consider the NEUS, which includes Maine, New Hampshire, Vermont, Massachusetts, Rhode Island, Connecticut, New York, New Jersey, Pennsylvania, Delaware, Maryland, West Virginia, and the District of Columbia, consistent with the previous studies of Frei et al. (2015), Huang et al. (2017), Agel et al. (2020), and Agel and Barlow (2020) (see Fig. 1 for an illustration of this region). Only surface variables are publicly available.

We use the bias-corrected NA-CORDEX output, which was obtained by the NA-CORDEX team (McGinnis and Mearns 2021) using the Cannon (2018) multivariate quantile-mapping algorithm against the gridded, daily Daymet observational dataset (which itself is based on observations from the Global Historical Climatology Network). Such bias correction is accepted practice for refining model data to analyze climate change impacts (Kirchmeier-Young et al. 2017; Zscheischler et al. 2018) and we refer the interested reader to Cannon (2018) for more information on the bias-correction algorithm and Behnke et al. (2016) for the uncertainty in Daymet data over regions for which there are few GHCN stations. While this algorithm minimizes model bias, it does not completely remove all bias, and differences in model climatologies remain.

We use all NA-CORDEX simulations that have publicly available, daily averaged, Daymet-corrected temperature and precipitation data spanning 1950–2100. All calculations are performed with daily averaged data, and throughout the analysis we take the "historical" period to be 1986–2005 and the "projected" period to be 2081–2100. Unless otherwise stated, we refer to the change in a variable as the difference between its average value during the projected period and its average value during the historical period. Simulations of future climate follow the RCP8.5 forcing scenario (i.e., the high emissions representative concentration pathway; Hausfather and Peters 2020), which most closely aligns with recent observations of both CO_2 emissions (Schwalm et al. 2020) and extreme precipitation (Lopez-Cantu et al. 2020). Furthermore, there are more simulations run using RCP8.5 than RCP4.5 in the NA-CORDEX ensemble, allowing us to conduct a more thorough analysis. Since the fractional change in extreme precipitation is not dependent on the emissions scenario (Pendergrass et al. 2015), we do not expect this choice to have a significant impact on our results.

We have investigated the role of internal variability by considering different historical and projected periods and find that all results presented below are qualitatively robust to the 20-yr spans chosen for the historical and projected periods (we also considered the similarly spaced periods of 1950–69 and 2045–64, not shown). Hence, while there is certainly internal variability present in the system (Huang et al. 2021), the century-scale extreme precipitation trends calculated here are primarily driven by the prescribed RCP8.5 forcing scenario, consistent with previous modeling studies (Agel et al. 2020; Agel and Barlow 2020).

There are 12 simulations (i.e., unique pairings of GCMs and RCMs) that match the selected spatial–temporal resolutions, bias-correction, and emissions scenario (Table 1). We have disregarded one of the simulations (CanESM2, CanRCM4) in most of our analysis, as this simulation is a clear outlier in the magnitude of the fractional change in extreme precipitation—the fractional change diagnosed from the CanESM2–CanRCM4 simulation is double that diagnosed from the average of the other 11 ensemble members (discussed further in section 3c). Additionally, Karmalkar (2018) found that the CanESM2–CanRCM4 simulation was the only NA-CORDEX simulation for which the downscaled precipitation was greater than the driving model. We have not investigated this pairing further but note that it is the only pairing that uses CanRCM4. The ensemble considered here is larger than those in previous dynamical downscaling studies (Hayhoe et al. 2008; Rawlins et al. 2012), allowing us to better quantify uncertainty.

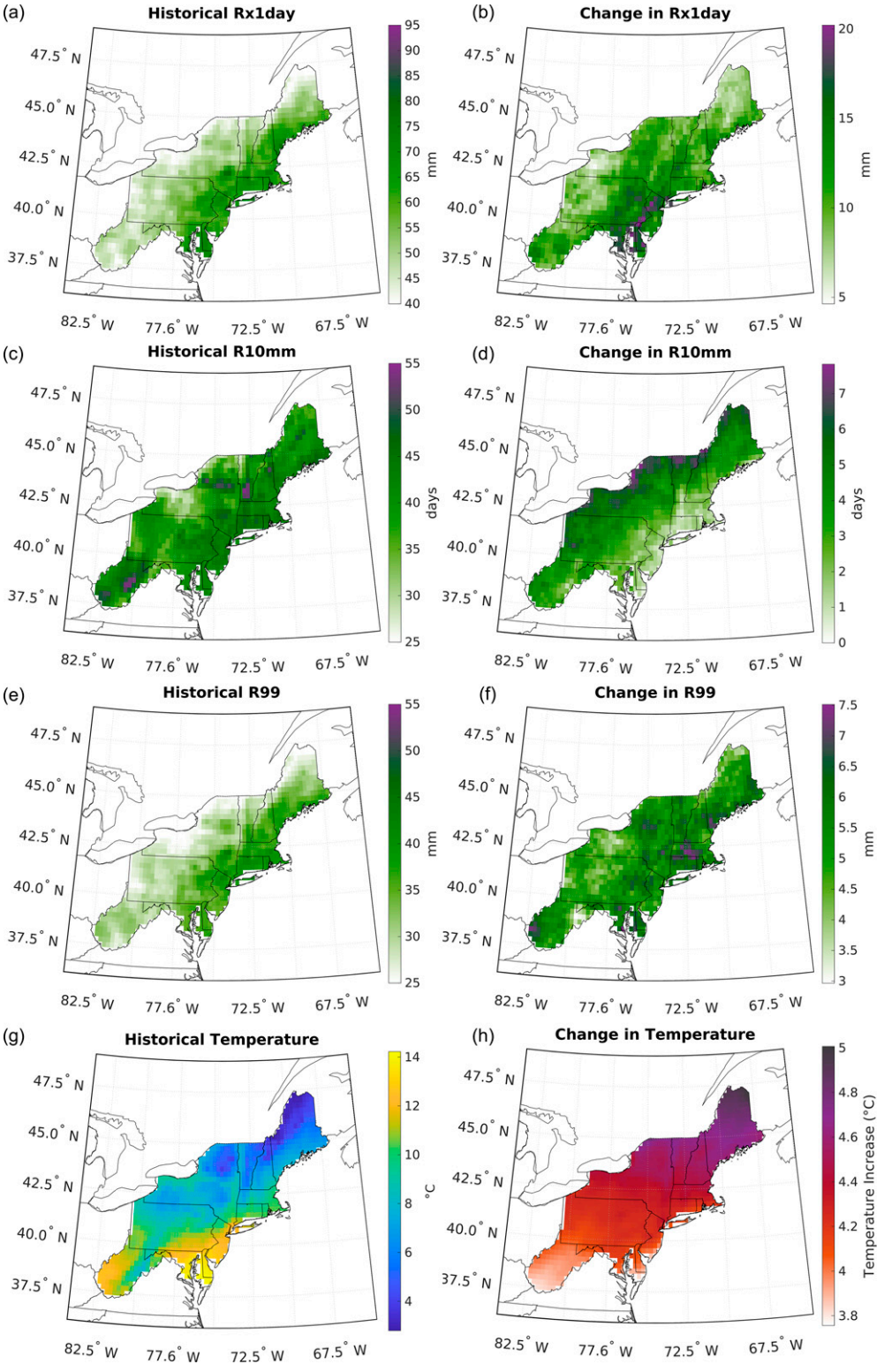

FIG. 1. (left) Historical and (right) change in extreme precipitation [as quantified by (a),(b) Rx1day; (c),(d) R10mm; and (e),(f) R99] and (g),(h) temperature. There is relatively good agreement in the historical Rx1day and R99 metrics [given in (a) and (e), respectively], with extreme precipitation having a coastal dependence, as is also the case in (b) and (f), showing the change in indices.

TABLE 1. Global and regional model pairings comprising the 12 available NA-CORDEX simulations with daily, bias-corrected output at 0.22° (~25 km) resolution and forced using RCP8.5. The equilibrium climate sensitivity (ECS; the temperature change due to a doubling of CO_2), as diagnosed by the NA-CORDEX team (see https://na-cordex.org/simulation-matrix.html and references therein), is noted for each model. The ECS is the same for each regional model associated with a given global model.

Global model	Regional model	ECS (°C)
CanESM2	CanRCM4; CRCM5-UQAM	3.7
GEMatm-Can	CRCM5-UQAM	3.7
GEMatm-MPI	CRCM5-UQAM	3.6
GFDL-ESM2M	RegCM4; WRF	2.4
HadGEM2-ES	RegCM4; WRF	4.6
MPI-ESM-LR	CRCM5-UQAM; RegCM4; WRF	3.6
MPI-ESM-MR	CRCM5-UQAM	3.4

As stated in section 1, the range of climate sensitivities in the NA-CORDEX ensemble is advantageous, as earlier studies used models with a much smaller range of sensitivities (Karmalkar 2018). For the 11 ensemble members used here, the equilibrium climate sensitivity ranges from 2.4° to 4.6°C [for reference, the equilibrium climate sensitivity of the full CMIP5 ensemble ranges from 2.0° to 4.7°C (Andrews et al. 2012; Flato et al. 2013)]. The spread in annual-mean North American precipitation projections from the downscaled NA-CORDEX simulations is greater than that of the driving GCMs alone and closer to that of the full CMIP5 ensemble (Bukovsky and Mearns 2020). Regardless of the global or regional model used, all simulations slightly overestimate the magnitude of average annual precipitation over the region (1.156 m, based on data from the Global Historical Climatology Network). Bukovsky and Mearns (2020) previously showed that the NA-CORDEX overestimates precipitation, similar to other ensembles (Rawlins et al. 2012), although the dynamical-downscaling of GCMs with RCMs does minimize the overestimation in precipitation. All 11 simulations are given equal weighting (i.e., all model projections are considered equally likely) in calculating the ensemble average for all diagnostic presented in section 3.

b. *Extreme precipitation indices and scaling*

Extreme precipitation can be quantified using a number of metrics, including the annual maximum of daily precipitation (Rx1day), the number of a days in a year with precipitation exceeding 10 mm (R10mm), and the 99th percentile of precipitation (R99) (Schar et al. 2016). After presenting a brief comparison of the metrics in Fig. 1, we will generally use R99 to quantify extreme precipitation throughout our analysis to be consistent with previous studies of regional extreme precipitation (Huang et al. 2017; Agel et al. 2018). Also consistent with earlier global modeling studies, we calculate extremes using all days (Ban et al. 2015; O'Gorman 2015), rather than wet days only, since the wet-day frequency does not necessarily remain fixed in a warming climate [see section 2c and also Schar et al. (2016)].

In presenting spatial data, the metrics are calculated at each grid box for each model, then averaged over the 11 ensemble members to create ensemble-mean maps. For the frequency analysis, daily, regionally averaged (weighted by area) precipitation is calculated for each model and R99 is taken from this time series. Values of R99 are then averaged across the 11 simulations to derive the ensemble average. Throughout this study, we calculate fractional changes in extreme precipitation (i.e., the percent change in R99 per degree warming), using local, rather than global, warming. While previous studies have calculated this ratio using global-mean warming, we instead use local warming so as to provide regional stakeholders with a more intuitive and localized planning metric. Moreover, we believe that local temperature is more informative for diagnosing the drivers of precipitation changes at the regional scales considered here, although local/regional changes in temperature are often more uncertain than global changes in temperature.

c. *Power-law distributions*

A convenient method of diagnosing changes in the frequency and intensity of extreme precipitation is to fit power-laws to the probability density functions (PDFs) of daily precipitation. We follow the method of Martinez-Villalobos and Neelin (2019) to do this, in which the PDFs of daily precipitation p are calculated as

$$\mathrm{PDF} = Ap^{-\tau}\exp(-p/P), \tag{1}$$

where $A = \Gamma(1-\tau)^{-1}P^{\tau-1}$, Γ is the gamma function, τ is the power-law exponent, and P is the cutoff scale. The value of τ represents the probability of light and moderate precipitation days, and the value of P represents the probability of extreme precipitation days. Taking the logarithm of (1) gives

$$\log(\mathrm{PDF}) \sim C_1 + C_2\log(p) + C_3p, \tag{2}$$

where $\tau = -C_2$ and $P = -C_3^{-1}$. The coefficients C_1, C_2, and C_3 can be obtained by linearly regressing the regionally averaged, daily precipitation onto the binned probabilities and then using (2) to obtain τ and P. Once this power-law fit has been performed for each simulation, we average the individual simulations' power-law exponents τ and cutoff scales P to derive the ensemble-averaged power-law distribution. This process is completed twice, once for the historical period (giving τ_H and P_H) and once for the projected period (giving τ_P and P_P), to diagnose regional changes in the frequency of extreme precipitation. A detailed explanation of daily precipitation distributions and a test of this distribution is provided in Martinez-Villalobos and Neelin (2019).

3. Results

a. *Ensemble-mean, annual-mean changes*

We begin by considering ensemble-mean changes across the NEUS. Averaged over the 11 ensemble-members, the NEUS experiences an annual-mean warming of 3.8°–5°C by the end of the twenty-first century, with the largest warming

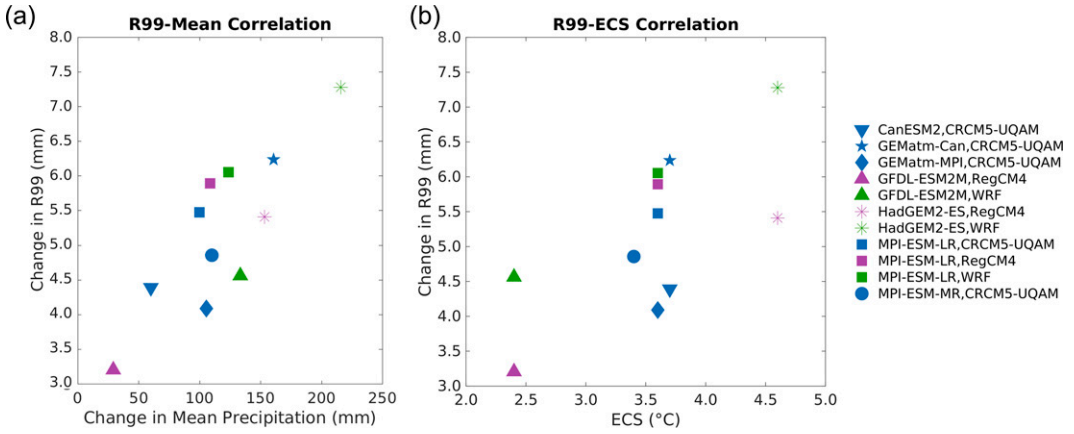

FIG. 2. (a) Correlation between the change in mean precipitation and the change in extreme precipitation (R99). (b) Correlation between the simulations' equilibrium climate sensitivity (ECS) and change in NEUS-average extreme precipitation (R99).

at higher latitudes (Fig. 1h; for reference, the globally averaged warming across the driving models is 2.4°–4.1°C). This latitudinal gradient in warming is consistent with prior studies of the NEUS (Hayhoe et al. 2008; Rawlins et al. 2012) and with the more general Arctic amplification of warming seen throughout the Northern Hemisphere in climate projections (e.g., Pithan and Mauritsen 2014). The simulations, however, do not capture the increased warming along the coast, as seen in the recent analysis of Karmalkar and Horton (2021).

Changes in extreme precipitation do not exhibit such a clear latitudinal gradient. Instead, the changes in both Rx1day and R99 are largest in coastal regions and smaller farther inland (Figs. 1b,f). Eastern Pennsylvania and New Jersey are projected to experience increases in Rx1day of up to 20 mm day^{-1}, while southern Massachusetts is projected to see increases in R99 of 7.5 mm day^{-1}. These patterns reflect the simulated and observed historical patterns of Rx1day and R99, which are also largest in coastal regions (Figs. 1a,e), consistent with Huang et al. (2017). However, for Figs. 1c,d R10mm, there is less of a coastal dependence, and a stronger coupling with orography, with peaks in extreme precipitation over mountain regions, such as the Appalachian, Adirondack, Green, and White Mountains. For Rx1day and R99, the presence of orographically driven precipitation is less pronounced. The relative agreement in the sign and spatial pattern of changes in Rx1day and R99 over the NEUS shown here is consistent with the analysis of Sillmann et al. (2013), who noted that the NEUS is one of the few regions where there is agreement among these indices in diagnosing trends in extreme precipitation.

Averaged over the region, R99 increases by approximately 5.7 mm (with a standard deviation of 0.3 mm), and the change is correlated across the ensemble with the change in mean precipitation (see Fig. 2a), as has been seen in projections of extreme precipitation in downscaled simulations of other regions (Nishant and Sherwood 2021). This change in R99 corresponds to an increase of approximately 20% between the historical and projected periods (separated by 95 years), which yields an increase in extreme precipitation of ~2% decade^{-1}, consistent with the historical rate of increase (Hoerling et al. 2016). That the rate of change is robust regardless of the time period considered suggests that the long-term anthropogenically induced warming is more important than climate variability in establishing extreme precipitation trends over the region on multidecadal time scales, which is consistent with the results of Pendergrass et al. (2015).

R10mm exhibits the opposite spatial pattern to the other two metrics, with the smallest increases in coastal regions and the largest increases farthest inland (Fig. 1d). To explain this pattern, Fig. 3a shows a power-law fit to the regionally averaged daily precipitation over the historical and projected time periods. Increases are seen in the occurrence of days with very low precipitation (<1 mm) and in the days with extreme precipitation days (>10 mm), while the number of days with moderate precipitation is projected to decrease. Note that Wang et al. (2020) found disagreement in the change in extreme precipitation frequency in their statistically downscaled ensembles, but the NA-CORDEX simulations show good agreement in the change in frequency.

Increases in the frequency of high precipitation days are seen at individual locations as well, and so, since 10 mm day^{-1} is a moderate rate of precipitation in coastal regions (Fig. 3b) and a more extreme rate inland (Fig. 3c), the largest changes in R10mm are seen in inland regions. The increase in occurrence of days with extreme precipitation is particularly notable in Fig. 3a, as the frequency of the strongest events increases by as much as a factor of 5 relative to the historical simulations. The 90% confidence intervals further underscore the robustness of these increases.

As a different way of showing the increase in the number of strong precipitation events, Fig. 4 plots the ensemble-averaged increase in frequency at different percentiles of the control climate. This can also be thought of as the increase in frequency of a particular return time relative to the control climate (i.e., a 1-in-10-yr event in the control climate becomes approximately 80% more likely by the end of the twenty-first

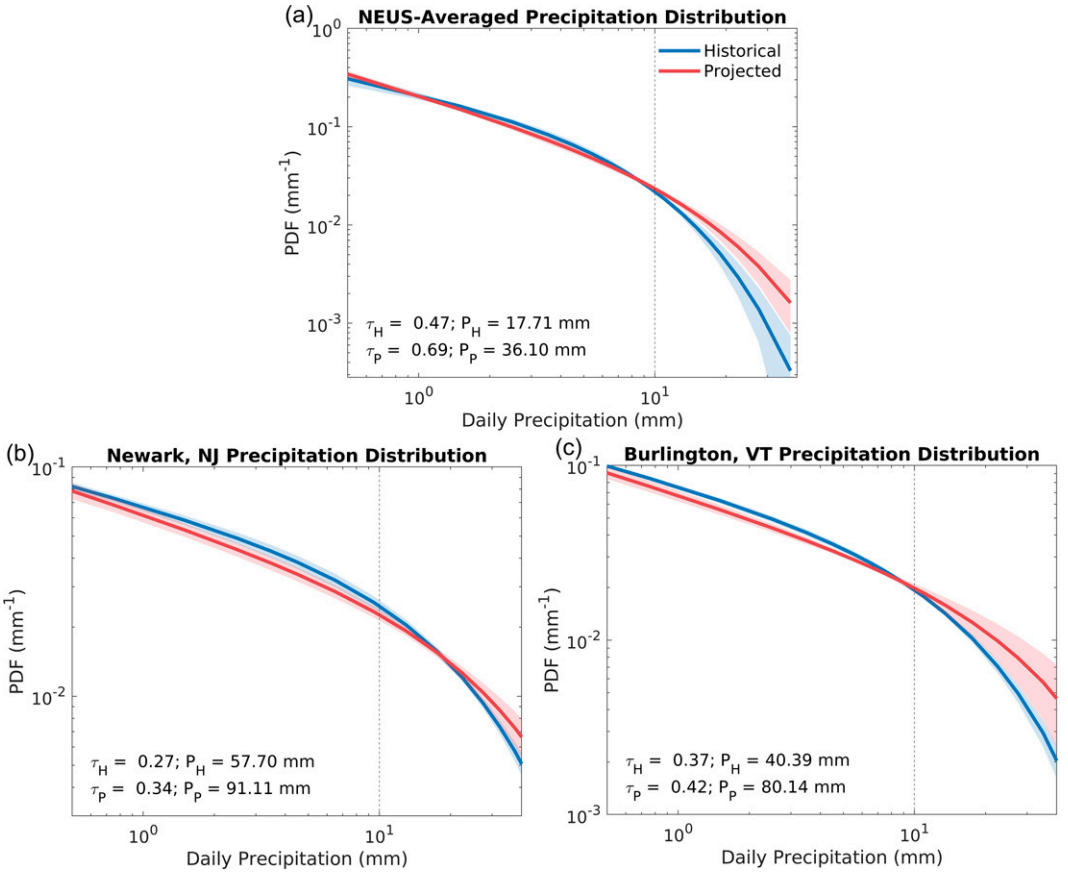

FIG. 3. Ensemble-averaged power-law distribution of daily precipitation from the 20-yr historical (blue) and projected (red) periods for (a) the entire NEUS; (b) Newark, New Jersey (40.74°N, 74.17°W), a typical coastal location; and (c) Burlington, Vermont (44.48°N, 73.21°W), a typical inland location. Shading indicates the 90% confidence interval. Note that the scales of the vertical axes vary in each panel.

century for each degree of warming). Given a temperature increase of approximately 5°C (Fig. 1h), Fig. 4 indicates a factor-of-5 increase in the frequency of the strongest storms, consistent with Fig. 3a [this result is likewise consistent with Allen and Ingram (2002), Walsh et al. (2014), and Myhre et al. (2019), among others].

b. *Seasonal changes*

We now discuss changes in extreme precipitation over the seasonal cycle, focusing on the R99 metric. The pattern of extreme precipitation changes is generally similar throughout the year (Fig. 5b,d,f,h), with the exception of summer [June–August (JJA)], when the increases in R99 are smaller and exhibit an inland intensification rather than a coastal intensification. In the historical simulations the magnitude and pattern of extreme precipitation in JJA is comparable to other seasons (see Fig. 5), and we have been unable to identify what causes the difference in the summer response when compared with the other seasons. We note that there is significant intermodel spread during summer (see section 3d), which suggests that models struggle to capture the changes in convective precipitation, which is common over the NEUS during the summer (see section 4 for further discussion).

The largest increase in extreme precipitation is seen in winter [December–February (DJF)], when a large swath of coastal NEUS sees increases of up to 8 mm day^{-1} in R99. Similarly large increases are seen in spring (MAM) and, for only some inland regions, fall (SON). We speculate that the processes that lead to enhanced wintertime precipitation, such as extratropical cyclones and frontal systems, which is clearly enhanced (Fig. 5b), may also be occurring more during the shoulder seasons (spring and fall), but further study is required. Given the spatial pattern of fall extreme precipitation trends (Fig. 5h), we do not expect that increases in tropical cyclone-driven extreme precipitation is driving this increase (this is discussed further in section 4).

Figure 6 shows the seasonal cycles of mean and extreme precipitation averaged over the NEUS region. Consistent with Fig. 5, the largest increases in both metrics are seen in winter/spring (November–May) and the smallest increases are seen in summer/early fall (June–September). However, the ensemble-spread in both monthly mean and extreme precipitation is large, and the changes are not statistically significant

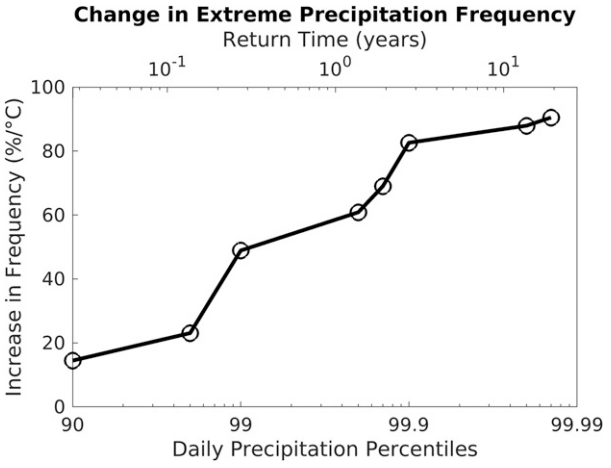

FIG. 4. Ensemble-averaged change in storm frequency (as measured through various percentiles) per degree Celsius of local warming. Corresponding return times are noted; for example, the change in the frequency of the (historical) 99.9 percentile storm is equivalent to the change in frequency of the ~1-in-3-yr storm. While not shown here, there is larger intermodel spread for higher percentiles, given the increasingly small sample size.

when averaged over the region. Despite the intermodel spread, Fig. 6 is reasonably consistent with seasonality results from earlier studies of regional trends (Hayhoe et al. 2008; Rawlins et al. 2012).

c. *Drivers of changes in extreme precipitation*

Extreme precipitation is generated by strong updrafts, such that the rate of extreme precipitation P_e can be approximated as

$$P_e \approx \int -\rho w\left(\frac{dq_s}{dz}\right)dz, \tag{3}$$

where ρ is the air density, w is the vertical velocity, q_s is the saturation specific humidity, and z is the vertical coordinate. We ignore changes in precipitation efficiency, which measures the efficiency with which cloud condensation is converted into precipitation. Precipitation efficiency, particularly of extreme precipitation, is an active area of research (see, e.g., Singh and O'Gorman 2014; Langhans et al. 2015; Lutsko and Cronin 2018; Abbott et al. 2020), and it is difficult to compare across models with different microphysics schemes, particularly given the available data for NA-CORDEX. However, we caution that what we infer to be dynamical changes may actually reflect undiagnosed changes in cloud microphysics.

This expression can be used to decompose fractional changes in P_e as

$$\frac{\delta P_e}{P_e} = \underbrace{\left[\frac{\int \rho w \delta\left(\frac{dq_s}{dz}\right)dz}{\int \rho w\left(\frac{dq_s}{dz}\right)dz}\right]}_{\text{thermodynamic}} + \underbrace{\left[\frac{\int \delta(\rho w)\left(\frac{dq_s}{dz}\right)dz}{\int \rho w\left(\frac{dq_s}{dz}\right)dz}\right]}_{\text{dynamic}} + \underbrace{\left\{\frac{\int \delta\left[\rho w\left(\frac{dq_s}{dz}\right)\right]dz}{\int \rho w\left(\frac{dq_s}{dz}\right)dz}\right\}}_{\text{nonlinear}}, \tag{4}$$

where δ is the difference between the projected and historical periods. The first term is the thermodynamic contribution to the change in extreme precipitation that, from the Clausius–Clapeyron relation, is approximately +6%–7% °C^{-1}. The second term is the contribution from dynamical changes and is typically ± 2% °C^{-1}. The final term is the contribution from nonlinear changes and is typically an order of magnitude smaller than the other two terms. As mentioned in section 2b, all fractional changes will be taken with respect to local, rather than global, temperature change. We cannot explicitly calculate the individual terms in (4) since only surface-level data are publicly available and individual modeling centers were only able to provide data at a few vertical levels, which is insufficient to calculate the vertical integrals.

Most of the NEUS experiences fractional increases in extreme precipitation of 2%–5% °C^{-1}, with a regional average increase of 3.6% °C^{-1} (Fig. 7a). This is consistent with previous global modeling studies showing that increases in extreme precipitation generally fall below the Clausius–Clapeyron value of 6%–7% °C^{-1} in the extratropics (Kharin et al. 2013; O'Gorman 2015). Additionally, the Clausius–Clapeyron rate is less than 7% °C^{-1} when using local warming rather than global warming, but still larger than the fractional increases seen here.

The smaller fractional increases in the NEUS suggest that dynamical changes—decreases in the speed of updrafts associated with extreme precipitation events—damp the changes in extreme precipitation. Given the lack of publicly available data at different atmospheric levels, we have not been able to investigate these changes further but note that a decrease in the dynamical contribution is at odds with a recent modeling study that showed that storm updrafts will increase (particularly for the strongest storms) in a warming climate (Tamarin-Brodsky and Hadas 2019). The importance of circulation changes in driving changes to vertical velocity was previously shown in the idealized simulations of Pendergrass et al. (2016) and Pendergrass and Gerber (2016).

Interestingly, the fractional changes in R99 exhibit a strong latitudinal dependence, with the smallest fractional changes in the northeastern part of the region (Maine, eastern New Hampshire, and eastern Massachusetts) and the largest fractional changes in the southwestern portion of the region (southwest Pennsylvania and West Virginia) as well as upstate New York (Figs. 7b,c; note that this pattern is also qualitatively consistent across seasons; see Fig. 8). This is the opposite of the temperature response and leads to a relatively latitudinally homogeneous change in extreme precipitation (Fig. 1f). Changes in extreme precipitation depend on the changes in temperature associated with individual storms, rather than changes in mean temperature. The former may be more spatially homogeneous than the latter, which would produce a more spatially homogeneous distribution of δP_e. We return to this point in the discussion of section 4.

d. *Intermodel spread*

The intermodel spread in the response of regionally averaged annual-mean R99 is linked to the models' climate

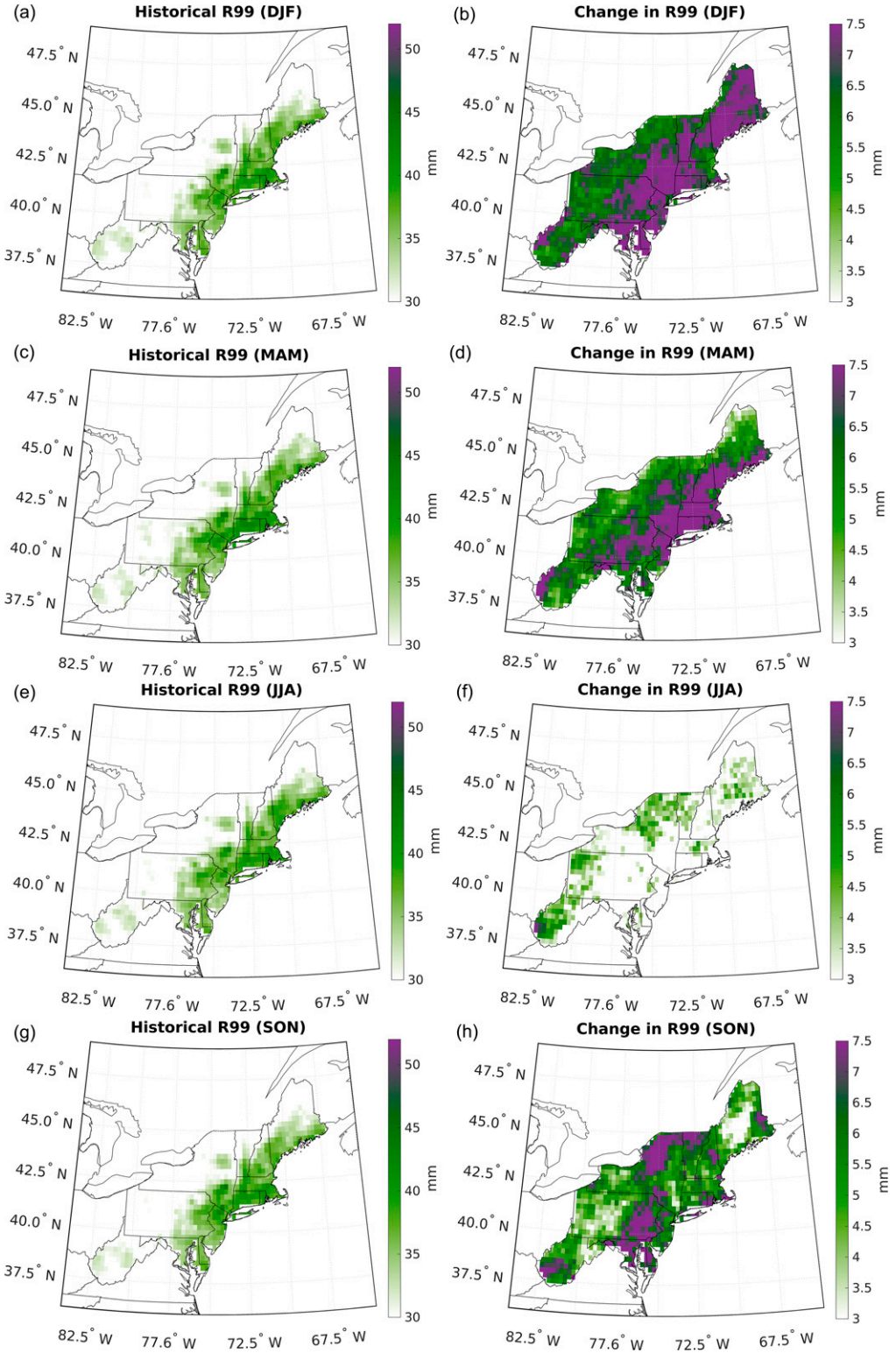

FIG. 5. As in Fig. 1e and 1f, but now considering the (a),(b) winter; (c),(d) spring; (e),(f) summer; and (g),(h) fall (left) historical and (right) change in extreme precipitation (R99).

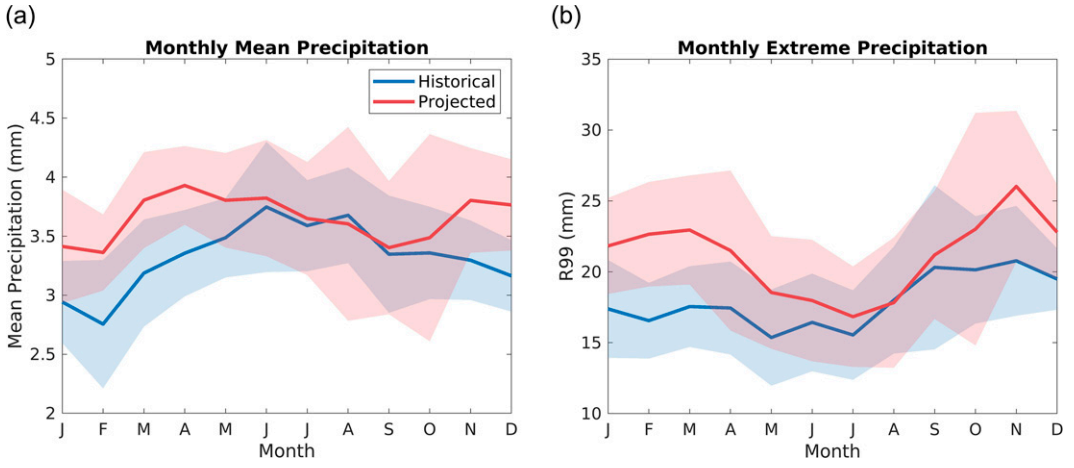

FIG. 6. (a) Average monthly mean precipitation, and (b) average monthly extreme precipitation, measured using R99, over the (blue) historical and (red) projected periods. Shading indicates the 90% confidence intervals.

sensitivities: more sensitive models produce larger increases in R99 over the NEUS (Fig. 2b). However, the NA-CORDEX ensemble members show good agreement in the magnitude of the fractional change in R99, with an ensemble-mean value of 3.6 with a standard error of 0.2% $°C^{-1}$ (Fig. 9a). Other metrics of extreme precipitation, such as R99.5, Rx1day, and R10mm, give similar fractional changes (not shown).

The model spread in the fractional change of extreme precipitation is noteworthy for two reasons. First, the lack of correlation between mean precipitation and the fractional change in extreme precipitation (Fig. 9a) suggests that the changes over the NEUS are robust across the physical processes resolved in these downscaled simulations. Second, several previous studies have shown that global models give inconsistent (in magnitude and, in some locations, sign) extreme precipitation trends over different regions (Sillmann et al. 2013), yet all of the model pairings considered here give positive extreme precipitation trends, with a small spread in magnitude. Both of these reasons give confidence in our estimate of the fractional change of 3.6% ± 0.2% $°C^{-1}$ over the NEUS.

For the same GCM, the spread in extreme precipitation fractional change across the different regional model pairings is small, which suggests that the driving model is primarily responsible for the extreme precipitation trend (see, for instance, the HadGEM2 ensemble members in Fig. 9a).

We consider the fractional change in extreme precipitation as a function of season and GCM–RCM pairing in Figs. 9b–e (see Fig. 8 for the corresponding plots of ensemble-averaged fractional change in extreme precipitation and Figs. 10b–e for the standard error in seasonal extreme precipitation). The model-averaged fractional changes for winter, spring, summer, and fall are 5.0%, 4.7%, 2.3%, and 2.7% $°C^{-1}$, respectively (if the change in temperature is small for a grid box, the regionally averaged change in temperature is used instead, so as to avoid unrealistically large fractional changes; this occurs in less than 5% of the grid boxes over all simulations). Figure 9 illustrates that, for all seasons, there is significantly more spread in the seasonal fractional change (and in R99, Figs. 10b–e) than in the annual-mean fractional change, with a couple models yielding negative fractional changes due to projected cooling during the shoulder seasons (MAM and SON). The HadGEM2-ES, RegCM4 simulation is not shown for spring (Figs 9c) since the fractional change is a large negative value due to unrealistic cooling.

While the annual extreme precipitation fractional change over the NEUS does not depend on the simulation's historical mean precipitation (Fig. 9a), Figs. 9c and 9d shows that the spring and summer extreme precipitation fractional change may be inversely related to the historical mean precipitation: for both of these seasons, simulations with lower historical seasonal precipitation experience a larger increase in extreme precipitation. All of the NA-CORDEX simulations overestimate mean annual and seasonal precipitation relative to that of the Global Historical Climatology Network (although not as much as the CMIP5 ensemble), which implies that the actual extreme precipitation fractional change may be larger than the means presented here given this inverse relationship. This would suggest that, while the absolute value of extreme precipitation increases the most during the winter and spring months (see Fig. 6), the fractional change in extreme precipitation is larger during the summer and fall, and closer in magnitude to the Clausius–Clapeyron scaling. This is consistent with recent downscaled simulations of Massachusetts that show the largest extreme precipitation fractional change occurring during the summer (Steinschneider and Najibi 2022).

In terms of the pattern of the extreme precipitation response, most ensemble members exhibit a coastal intensification of extreme precipitation (Fig. 11), although there are several members that show more homogeneous patterns of R99 change (i.e., GEMatm-Can, CRCM5-UQAM, and HadGEM2-ES, WRF). The standard error is roughly constant over the region (Fig. 10a) and is generally small in comparison with the change in extreme precipitation (approximately 15%). There are no parts of the NEUS in which the response

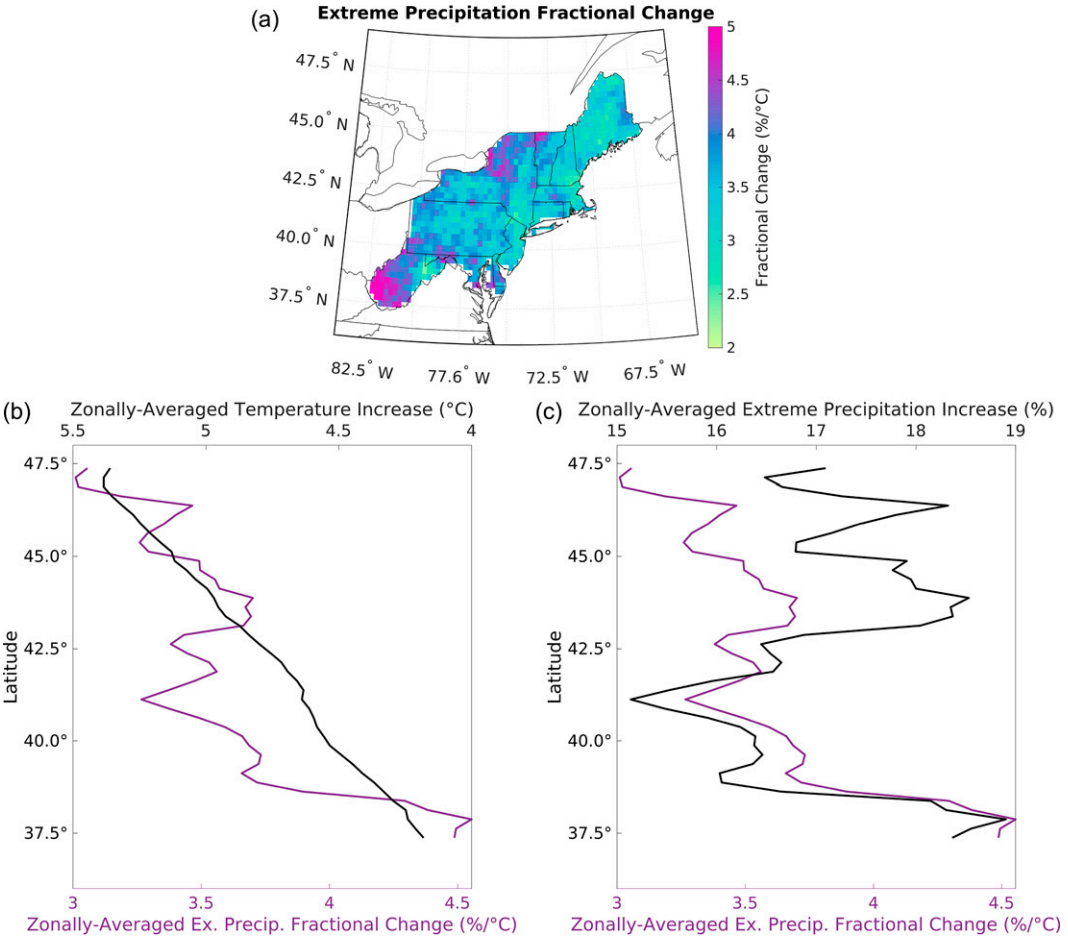

FIG. 7. (a) Fractional changes in ensemble-average extreme precipitation. Also shown are the zonally averaged (b) change in temperature and (c) percent change in R99 (black lines) plotted as a function of latitude, with the fractional change in extreme precipitation per degree Celsius superimposed (purple lines). Note the different scales for the horizontal axes at the top of (b) and (c).

of extreme precipitation seems to be especially uncertain. The intermodel spread in the change and fractional change in extreme precipitation is small during winter and spring (Figs. 9b,c and 10b,c) and significantly larger during summer and fall (Figs. 9d,e and 10d,e), suggesting that the processes responsible for the changes in extreme precipitation for these seasons (i.e., isolated convective systems and tropical cyclones) is poorly captured across the models.

The majority of the ensemble members likewise agree on the spatial pattern of the fractional change in annual precipitation (Fig. 12), with the largest values (~6% $°C^{-1}$) in the southwest portion of the region and upstate New York and the smallest values (~2% $°C^{-1}$) in the northeast portion of the region [the CanESM2 ensemble member (Fig. 12a), however, is not consistent with the spatial pattern of other 10 members].

4. Discussion and conclusions

In this study, we have used the NA-CORDEX ensemble to make the first comprehensive assessment of changes in extreme precipitation over the NEUS using a large suite of dynamically downscaled simulations encompassing a broad range of climate sensitivities. The use of high-resolution, dynamically downscaled simulations is essential for obtaining accurate and robust projections of future extreme precipitation at the scales required for planning and adaptation purposes.

Averaged over the region, we find that in the ensemble-mean the 99th percentile of daily precipitation (R99) increases by 5.7 ± 0.3 mm by the end of the twenty-first century under the RCP8.5 scenario, an increase of approximately 20% relative to the end of the twentieth century, or a rate of 3.6% $°C^{-1}$ of warming. This is consistent with the historical rate of increase of roughly 2% $decade^{-1}$ (Hoerling et al. 2016). Examining PDFs of regionally averaged, daily mean precipitation shows a general tendency for increases in the number of dry days and in days with heavy precipitation over the course of the twenty-first century, with relatively fewer days of moderate precipitation (~1–10 mm). While this is consistent with projections of precipitation in other midlatitude regions, which show a similar pattern of rainfall becoming

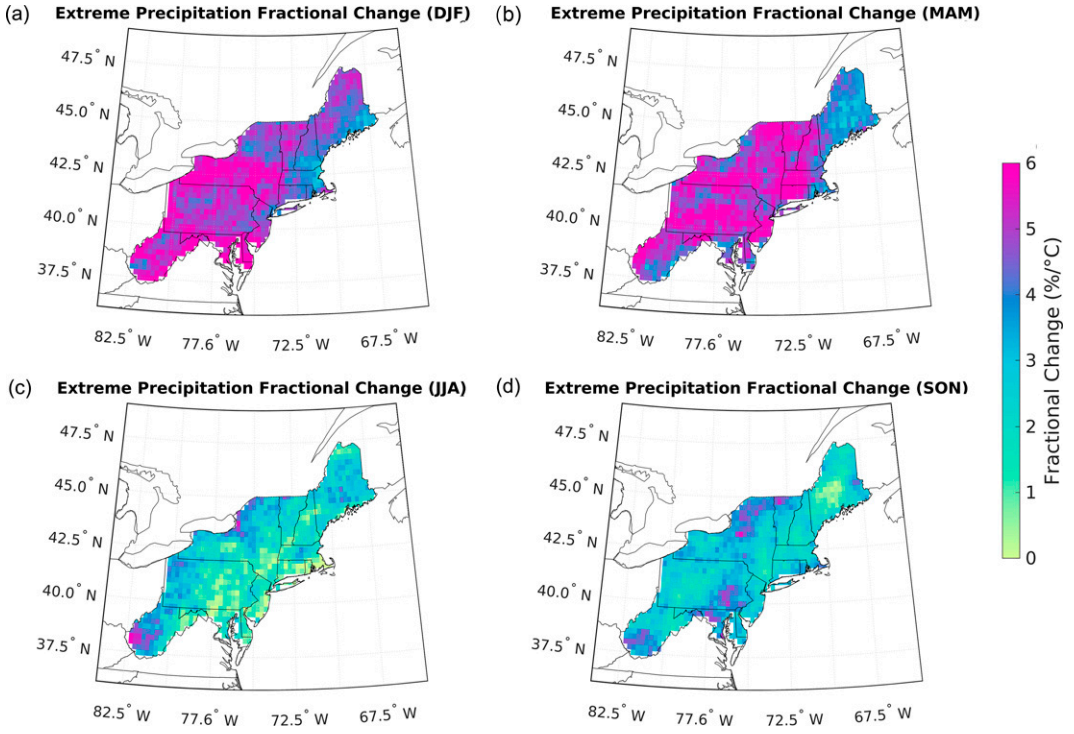

FIG. 8. As in Fig. 7a, but for (a) winter, (b) spring, (c) summer, and (d) fall.

more intermittent but more intense, this was not seen in the earlier, high-resolution simulations of the NEUS of Wang et al. (2020) and represents an advancement of our understanding of changes in extreme precipitation frequency. Relative to the end of the twentieth century, extreme precipitation events over the NEUS may become up to 5 times as frequent in the last decade of the twenty-first century.

The changes over the NEUS show a marked coastal intensification, with the largest increases in coastal regions (consistent with Thibeault and Seth 2014) and smaller increases occur farther inland. For instance, southern Massachusetts (coastal) is projected to see an increase in R99 of up to 7.5 mm day^{-1}, while parts of upstate New York (inland) may see increases of just 3 mm day^{-1}. This coastal intensification reflects the historical pattern of extreme precipitation.

The increases in R99 are not evenly distributed throughout the year; the smallest changes are generally seen in summer and, to a lesser extent, fall (see Figs. 5f, 6b, and 9d). This result contrasts with earlier observational studies that have shown the largest increases in extreme precipitation during the warm season (Frei et al. 2015) [note, however, that the seasonal changes are less robust, particularly when averaging over the entire region (see Figs. 6b and 10b)]. This result, coupled with the atypical inland spatial pattern of extreme precipitation change over summer (Fig. 5f) and the small increase in extreme precipitation over the start of the fall (Fig. 6) suggests that the NA-CORDEX ensemble may not fully capture the extreme precipitation associated with tropical cyclones over the NEUS, which are expected to lead to more coastal extreme precipitation (Garner et al. 2021). Rendfrey et al. (2021) used three WRF simulations from the NA-CORDEX ensemble (at 0.22°) and found that coastal portions of the region will experience an increase in tropical cyclone-associated annual precipitation of 20 mm yr^{-1}, although the results were not robust across the NEUS, and this is less than a third of the ensemble size considered in this study. The role of tropical cyclones and, in particular, the seasonality of extreme precipitation associated with tropical cyclones in NA-CORDEX warrants further study. Additionally, it is well documented that models (even at 0.22° resolution) poorly resolve convection, which is the primary driver of JJA extreme precipitation over the NEUS. Given the limited ability of models to capture convectively driven extreme precipitation, it is not surprising that simulations do not necessarily capture the change in summertime extreme precipitation seen in observations (Frei et al. 2015).

One of the benefits of conducting dynamical downscaling studies is the more realistic representation of precipitation due to surface forcing, such as orography. NA-CORDEX reasonably resolves historical orographic precipitation, particularly on the climatological windward side of mountains (see Fig. 1c), but, regardless of the metric, Figs. 1b,1d and 1e does not show notable changes in extreme precipitation in regions of significant orography (such as the Appalachian, Adirondack, Green, or White Mountains). Prior work suggests that the climatological leeward sides of mountains will experience increases in extreme precipitation in a warming climate (O'Gorman 2015, and references therein), but that is not seen in this ensemble of dynamically downscaled simulations and provides an avenue for further research as well as a potential metric for evaluating downscaled simulations.

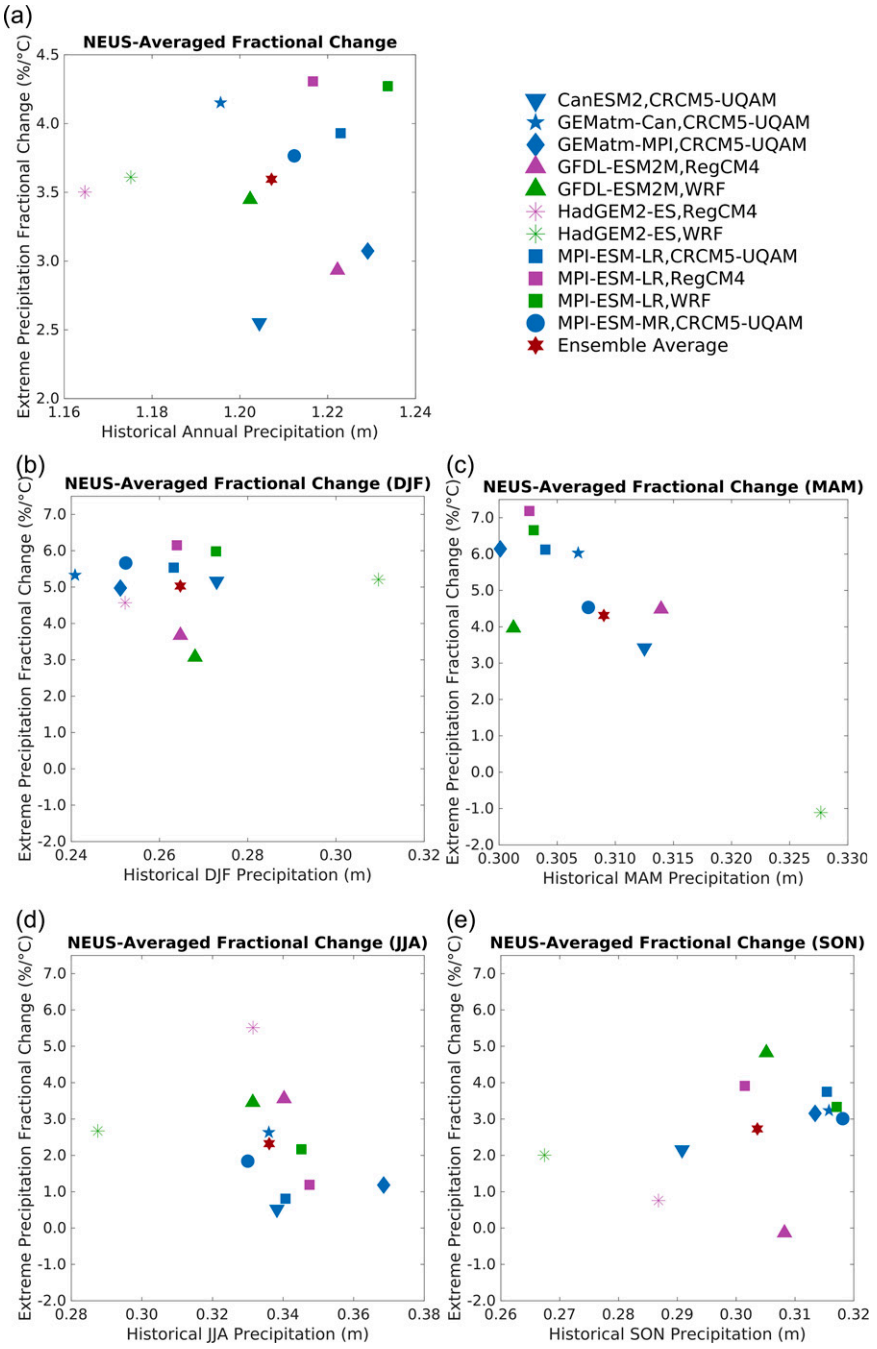

FIG. 9. The regionally averaged (a) annual, (b) winter, (c) spring, (d) summer, and (e) fall extreme precipitation fractional change for each of the 11 models considered in this study. Individual NA-CORDEX simulations (as well as the ensemble average) are labeled, with each global (i.e., driving) model having a unique symbol and each regional model having a unique color. Note the different vertical scale for the annual [in (a)] and seasonal [in (b)–(e)] fractional changes.

Furthermore, we have not considered the impacts of urbanization in this study or other dynamic land changes and associated feedbacks on extreme precipitation. Such analysis with CORDEX has been conducted for Africa (Soares et al. 2019), Europe (Knist et al. 2017), and the Middle East and northern Africa (Constantinidou et al. 2020) and was the primary focus of these studies. While we have not conducted a sweep of land surface schemes here, we expect that, based on the work

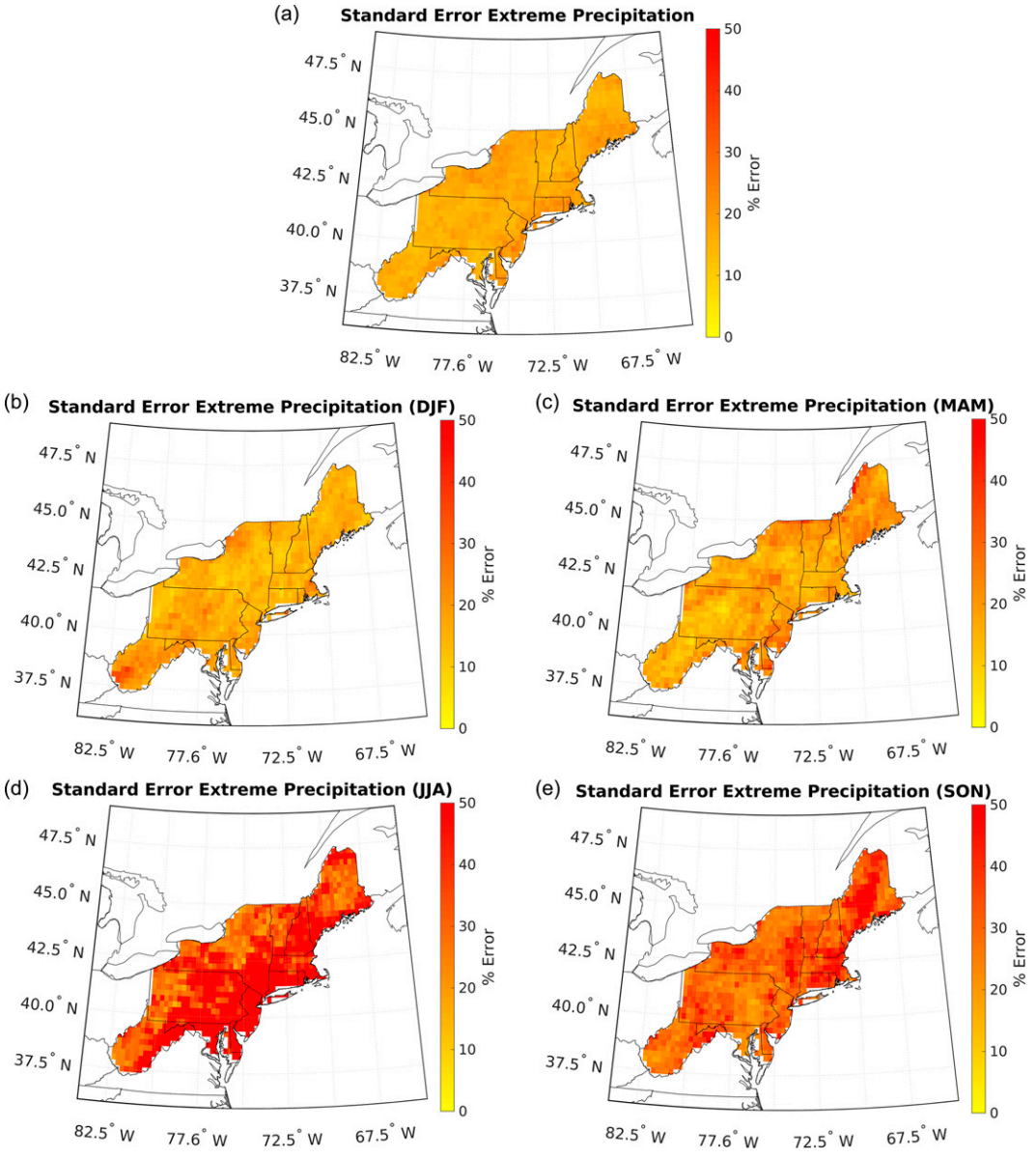

FIG. 10. The (a) annual, (b) winter, (c) spring, (d) summer, and (e) fall percent error in the change in R99 over the 11 ensemble members. To calculate the percent change, the standard error in R99 across the ensemble is normalized by the ensemble average change in R99 and multiplied by 100 at each grid box.

of Singh et al. (2020), urbanization would exacerbate the increase in extreme precipitation over much of the NEUS. Much of this region, particularly the coastal communities, are densely populated, which Singh et al. (2020) showed has an amplifying effect on extreme precipitation trends. If we continue to follow this high emissions scenario and the region continues to become more densely populated, the increases in extreme precipitation presented here for the NEUS may represent lower bounds on the actual increases.

Over most of the NEUS, extreme precipitation increases by 2%–5% per °C of local warming, which is less than would be expected from thermodynamic considerations alone and suggests that dynamical changes are damping the increase in extreme precipitation (as noted in section 2b, this difference is also due, in part, to considering the local rate, and not the global rate, of warming). Furthermore, this fractional change in extreme precipitation is seasonally dependent, with all seasons experiencing a sub-Clausius–Clapeyron increase; the largest change occurring in wintertime (approximately +5% $°C^{-1}$) and the smallest change in summer (approximately +2% $°C^{-1}$). Based on the publicly available output for NA-CORDEX, we cannot diagnose the causes of these dynamic changes, but a slowdown of updraft speeds associated with extreme precipitation events is implied in contrast to the

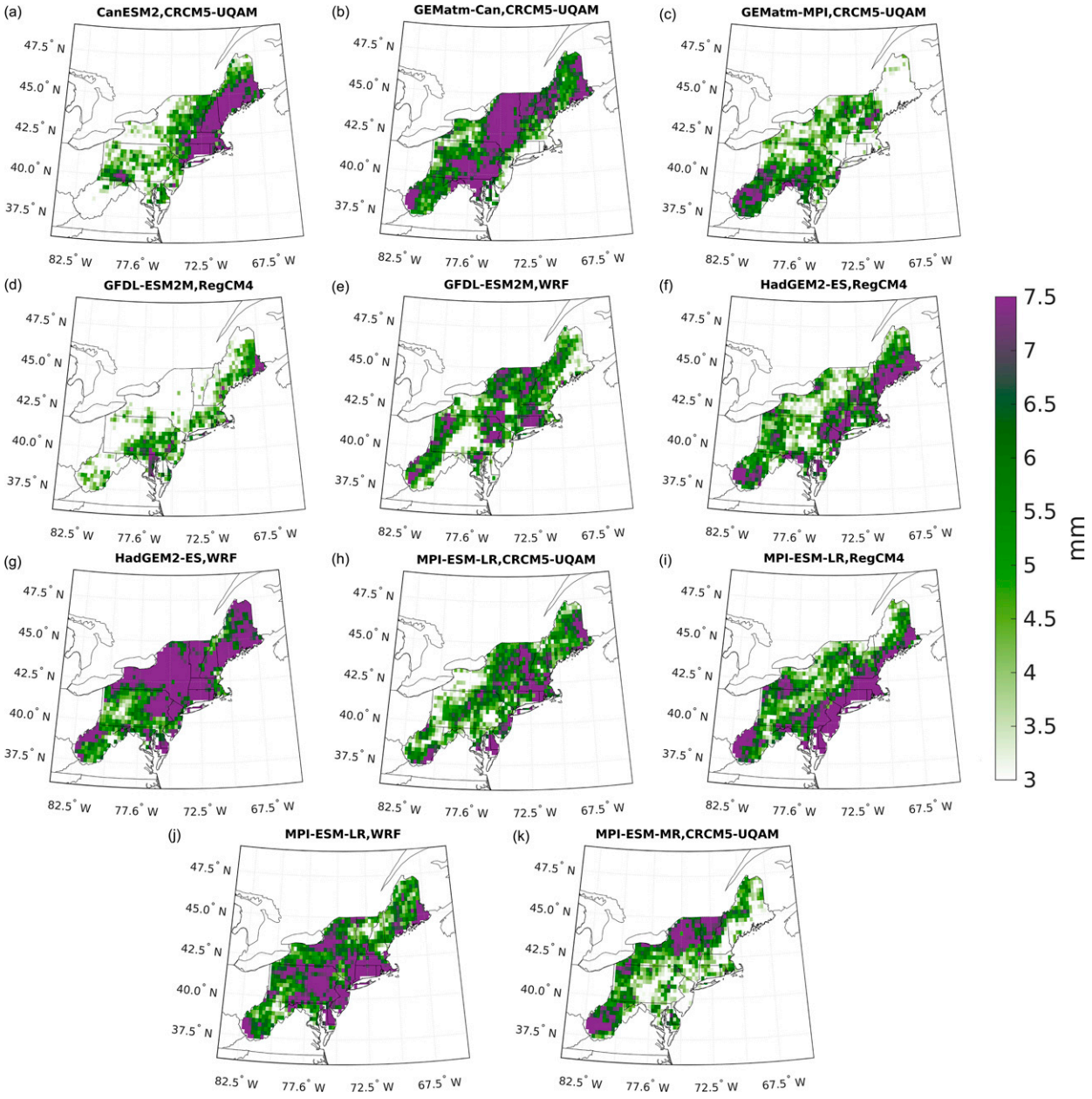

FIG. 11. Spatial distribution of the change in annual extreme precipitation (R99) for the 11 ensemble members considered in this study.

recent study of Tamarin-Brodsky and Hadas (2019). This is a novel result and warrants further study.

Note also that the temperature response exhibits a latitudinal gradient, such that higher latitudes warm more, but the changes in extreme precipitation do not show such a gradient. This means that the fractional changes in extreme precipitation are largest in the southern portion of the NEUS and smallest in the north. We interpret this as changes in extreme precipitation depending more on the temperatures associated with individual extreme events, rather than on changes in average temperatures, with the former more evenly distributed in latitude than the latter. However, at present it is unclear which temperatures to use when diagnosing the drivers of changes in extreme precipitation at the regional scale. Furthermore, the change in temperature diagnosed here lacks the coastal dependence seen in the recent model analysis of Karmalkar and Horton (2021), which warrants further study. Global- or regional-mean temperatures may not provide the entire story and, instead, detailed tracking of the storms that produce extreme precipitation in the NEUS will likely be needed to fully understand what drives the thermodynamically driven changes in extreme precipitation described here. While this is outside the scope of this study, we note that such a tracking is necessary to understand trends in extreme

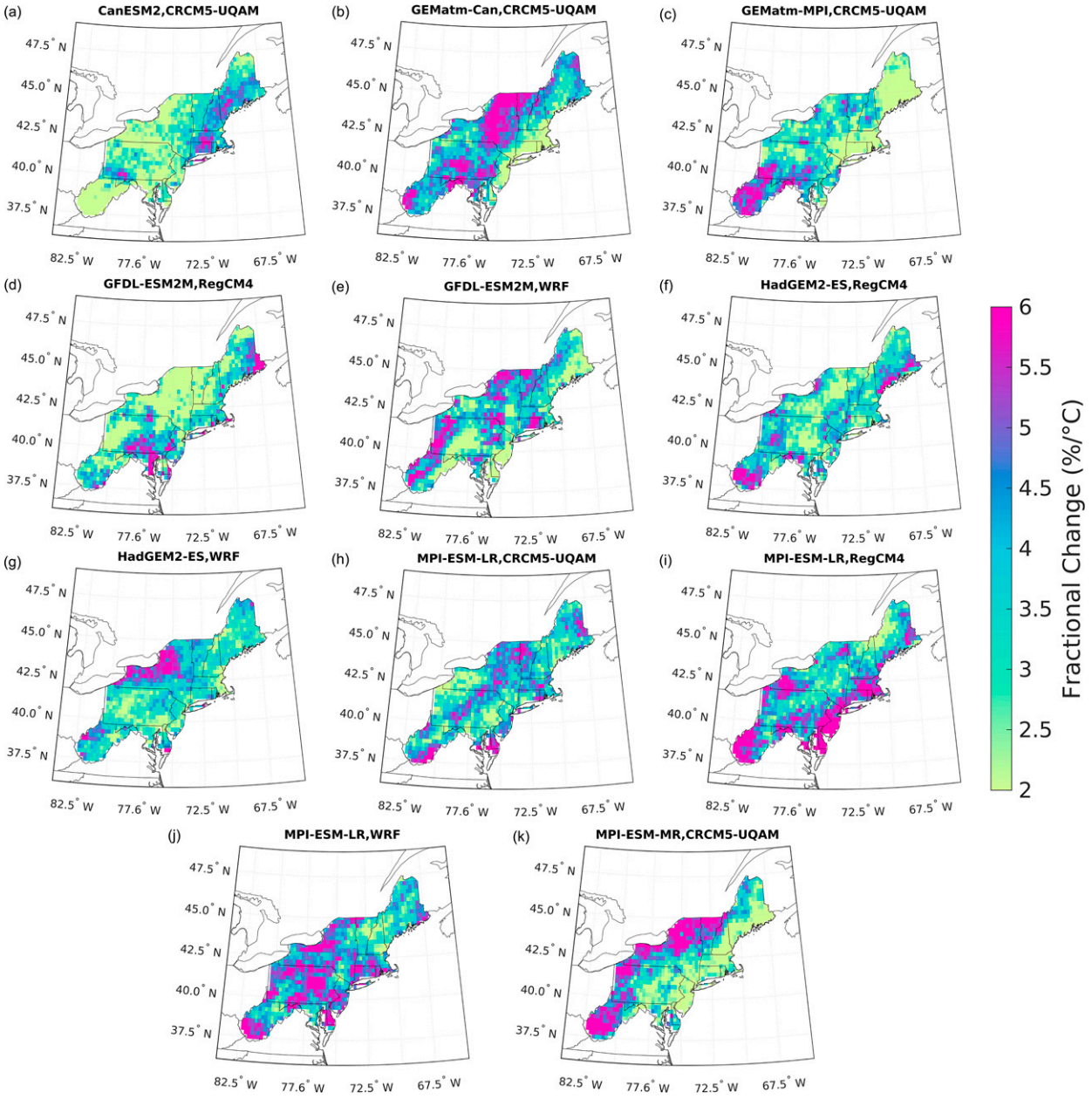

FIG. 12. Spatial distribution of the fractional change in annual extreme precipitation for the 11 ensemble members considered in this study.

precipitation over this region. Specifically, in the tropical atmosphere, we expect that the Clausius–Clapeyron relationship will hold locally, since most precipitation is due to convection, and the moisture is locally sourced. Most of the precipitation over the NEUS, however, is due to baroclinic storms, which pick up water over the mid-Atlantic and, based on the temperature, may yield a fractional change in extreme precipitation below the canonical 7% $°C^{-1}$. Understanding where the storms take up moisture, and how the temperature of these regions is changing, is of first-order importance in accurately diagnosing extreme precipitation trends over the NEUS. Nevertheless, in the interim, the fractional changes documented here may be of use to regional stakeholders who want to quantify the magnitude of the change in terms of the local rate of warming.

The ensemble members participating in NA-CORDEX generally show good agreement in the regionally averaged change in extreme precipitation, and most of the spread in the magnitude of the R99 response averaged over the region comes from ensemble members' equilibrium climate sensitivities. The ensemble members also generally agree on the qualitative pattern of the extreme precipitation response (i.e., the

coastal amplification). One exception is CanESM2–CanRCM4, which projects much larger increases in extreme precipitation than the other ensemble members, roughly following the scaling implied by the Clausius–Clapeyron relation. CanESM2–CanRCM4 is the only NA-CORDEX simulation for which the downscaled precipitation is greater than the driving model and is also the only pairing that uses CanRCM4. Given the good agreement between the other model pairings, we believe that this is an outlier simulation, and have chosen to disregard it in the majority of our analysis. More work is needed to identify what causes the anomalous behavior of this simulation.

We have not considered the type of precipitation and, more specifically, how snowfall over the region will change in a warming climate. Using observations, Kunkel et al. (2013) documented an increase in the frequency of extreme snowfall over the past several decades over the eastern United States. It is not clear that this trend will persist over the entire region through the end of the century, as the occurrence of temperatures below the rain-snow transition temperature may decrease (Diffenbaugh et al. 2013; O'Gorman 2014) despite the magnitude of extreme precipitation increasing during cold months (Fig. 6). Given our results that show that the NEUS will experience the largest increases in extreme precipitation during the winter months, follow up studies on the detailed mechanisms of this increase and the type of precipitation falling during this time are required, and the NA-CORDEX ensemble may prove fruitful.

In summary, this work demonstrates that the entire NEUS should expect to have more frequent and more intense extreme precipitation events, with the largest increases in extreme precipitation occurring closest to the coast. Important open questions remain concerning the contribution of changes in Atlantic hurricanes to extreme precipitation over the NEUS, the type of precipitation that will fall during the heavier wintertime extreme precipitation events, and the dynamical changes that seem to damp the increases in extreme precipitation in projections of the twenty-first century. These questions may require novel modeling and analysis approaches to address. In any case, resilience and adaptation planners should prepare for a NEUS that experiences substantial increases in the frequency and intensity of extreme precipitation.

Acknowledgments. Authors R. Nazarian, J. Vizzard, and C. Agostino gratefully acknowledge support from Fairfield University, including the College of Arts and Sciences, Science Institute, and Provost's Office. Nazarian, Vizzard, and Agostino also gratefully acknowledge support from the NASA Connecticut Space Grant Consortium, Award P-1704. Author N. Lutsko was supported by NSF Grant OCE-2023483. The authors thank the editor and three reviewers for their helpful feedback, Seth McGinnis and Katja Winger for help in accessing the NA-CORDEX data, and Kieran Bhatia for helpful comments on the presentation of the frequency analysis. More information about conducting undergraduate research with CORDEX can be found in Nazarian (2021).

Data availability statement. All NA-CORDEX simulations used in this study are freely available on the NCAR Climate Data Gateway (https://www.earthsystemgrid.org/search/cordexsearch.html).

REFERENCES

Abbott, T. H., T. W. Cronin, and T. Beucler, 2020: Convective dynamics and the response of precipitation extremes to warming in radiative–convective equilibrium. *J. Atmos. Sci.*, **77**, 1637–1660, https://doi.org/10.1175/JAS-D-19-0197.1.

Agel, L., and M. Barlow, 2020: How well do CMIP6 historical runs match observed northeast U.S. precipitation and extreme precipitation-related circulation? *J. Climate*, **33**, 9835–9848, https://doi.org/10.1175/JCLI-D-19-1025.1.

——, ——, J.-H. Qian, F. Colby, E. Douglas, and T. Eichler, 2015: Climatology of daily precipitation and extreme precipitation events in the northeast United States. *J. Hydrometeor.*, **16**, 2537–2557, https://doi.org/10.1175/JHM-D-14-0147.1.

——, ——, S. B. Feldstein, and W. J. Gutowski Jr., 2018: Identification of large-scale meteorological patterns associated with extreme precipitation in the US northeast. *Climate Dyn.*, **50**, 1819–1839, https://doi.org/10.1007/s00382-017-3724-8.

——, ——, J. Polonia, and D. Coe, 2020: Simulation of northeast U.S. extreme precipitation and its associated circulation by CMIP5 models. *J. Climate*, **33**, 9817–9834, https://doi.org/10.1175/JCLI-D-19-0757.1.

Alexander, L. V., and Coauthors, 2006: Global observed changes in daily climate extremes of temperature and precipitation. *J. Geophys. Res.*, **111**, D05109, https://doi.org/10.1029/2005JD006290.

Allen, M. R., and W. J. Ingram, 2002: Constraints on future changes in climate and the hydrologic cycle. *Nature*, **419**, 224–232, https://doi.org/10.1038/nature01092.

Andrews, T., J. Gregory, M. Webb, and K. Taylor, 2012: Forcing, feedbacks and climate sensitivity in CMIP5 coupled atmosphere–ocean climate models. *Geophys. Res. Lett.*, **39**, L09712, https://doi.org/10.1029/2012GL051607.

Ashfaq, M., D. Rastogi, R. Mei, S.-C. Kao, S. Gangrade, B. S. Naz, and D. Touma, 2016: High-resolution ensemble projections of near-term regional climate over the continental United States. *J. Geophys. Res. Atmos.*, **121**, 9943–9963, https://doi.org/10.1002/2016JD025285.

Ban, N., J. Schmidli, and C. Schar, 2015: Heavy precipitation in a changing climate: Does short-term summer precipitation increase faster? *Geophys. Res. Lett.*, **42**, 1165–1172, https://doi.org/10.1002/2014GL062588.

Bao, J., S. C. Sherwood, L. V. Alexander, and J. P. Evans, 2017: Future increases in extreme precipitation exceed observed scaling rates. *Nat. Climate Change*, **7**, 128–132, https://doi.org/10.1038/nclimate3201.

Behnke, R., S. Vavrus, A. Allstadt, T. Albright, W. E. Thogmartin, and V. C. Radeloff, 2016: Evaluation of downscaled, gridded climate data for the conterminous United States. *Ecol. Appl.*, **26**, 1338–1351, https://doi.org/10.1002/15-1061.

Bukovsky, M. S., and L. O. Mearns, 2020: Regional climate change projections from NA-CORDEX and their relation to climate sensitivity. *Climatic Change*, **162**, 645–665, https://doi.org/10.1007/s10584-020-02835-x.

Cannon, A. J., 2018: Multivariate quantile mapping bias correction: An *N*-dimensional probability density function transform

for climate model simulations of multiple variables. *Climate Dyn.*, **50**, 31–49, https://doi.org/10.1007/s00382-017-3580-6.

Constantinidou, K., P. Hadjinicolaou, G. Zittis, and J. Lelieveld, 2020: Performance of land surface schemes in the WRF model for climate simulations over the MENA-CORDEX domain. *Earth Syst. Environ.*, **4**, 647–665, https://doi.org/10.1007/s41748-020-00187-1.

Diffenbaugh, N. S., J. S. Pal, R. J. Trapp, and F. Giorgi, 2005: Fine-scale processes regulate the response of extreme events to global climate change. *Proc. Natl. Acad. Sci. USA*, **102**, 15 774–15 778, https://doi.org/10.1073/pnas.0506042102.

——, M. Scherer, and M. Ashfaq, 2013: Response of snow-dependent hydrologic extremes to continued global warming. *Nat. Climate Change*, **3**, 379–384, https://doi.org/10.1038/nclimate1732.

Di Luca, A., R. de Elia, and R. Laprise, 2012: Potential for added value in precipitation simulated by high-resolution nested regional climate models and observations. *Climate Dyn.*, **38**, 1229–1247, https://doi.org/10.1007/s00382-011-1068-3.

Fischer, E. M., U. Beyerle, and R. Knutti, 2013: Robust spatially aggregated projections of climate extremes. *Nat. Climate Change*, **3**, 1033–1038, https://doi.org/10.1038/nclimate2051.

——, J. Sedláček, E. Hawkins, and R. Knutti, 2014: Models agree on forced response pattern of precipitation and temperature extremes. *Geophys. Res. Lett.*, **41**, 8554–8562, https://doi.org/10.1002/2014GL062018.

Flato, G., and Coauthors, 2013: Evaluation of climate models. *Climate Change 2013 - The Physical Science Basis*, T. F. Stocker et al., Eds., Cambridge University Press, 741–866.

Frei, A., K. E. Kunkel, and A. Matonse, 2015: The seasonal nature of extreme hydrological events in the northeastern United States. *J. Hydrometeor.*, **16**, 2065–2085, https://doi.org/10.1175/JHM-D-14-0237.1.

Gandini, A., L. Garmendia, I. Alvarez, and J.-T. San-Jose, 2020: A holistic and multi-stakeholder methodology for vulnerability assessment of cities to flooding and extreme precipitation events. *Sustainable Cities Soc.*, **63**, 102437, https://doi.org/10.1016/j.scs.2020.102437.

Garner, A. J., R. E. Kopp, and B. P. Horton, 2021: Evolving tropical cyclone tracks in the North Atlantic in a warming climate. *Earth's Future*, **9**, e2021EF002326, https://doi.org/10.1029/2021EF002326.

Groisman, P. Ya., R. W. Knight, D. R. Easterling, T. R. Karl, G. C. Hegerl, and V. N. Razuvaev, 2005: Trends in intense precipitation in the climate record. *J. Climate*, **18**, 1326–1350, https://doi.org/10.1175/JCLI3339.1.

Hausfather, Z., and G. P. Peters, 2020: RCP8.5 is a problematic scenario for near-term emissions. *Proc. Natl. Acad. Sci. USA*, **117**, 27 791–27 792, https://doi.org/10.1073/pnas.2017124117.

Hayhoe, K., and Coauthors, 2008: Regional climate change projections for the northeast USA. *Mitigation Adapt. Strategies Global Change*, **13**, 425–436, https://doi.org/10.1007/s11027-007-9133-2.

Hoerling, M., J. Eischeid, J. Perlwitz, X.-W. Quan, K. Wolter, and L. Cheng, 2016: Characterizing recent trends in U.S. heavy precipitation. *J. Climate*, **29**, 2313–2332, https://doi.org/10.1175/JCLI-D-15-0441.1.

Howarth, M. E., C. D. Thorncroft, and L. F. Bosart, 2019: Changes in extreme precipitation in the northeast United States: 1979–2014. *J. Hydrometeor.*, **20**, 673–689, https://doi.org/10.1175/JHM-D-18-0155.1.

Huang, H., J. M. Winter, E. C. Osterberg, R. M. Horton, and B. Beckage, 2017: Total and extreme precipitation changes over the northeastern United States. *J. Hydrometeor.*, **18**, 1783–1798, https://doi.org/10.1175/JHM-D-16-0195.1.

——, ——, and ——, 2018: Mechanisms of abrupt extreme precipitation change over the northeastern United States. *J. Geophys. Res. Atmos.*, **123**, 7179–7192, https://doi.org/10.1029/2017JD028136.

——, C. Patricola, J. Winter, E. Osterberg, and J. Mankin, 2021: Rise in northeast US extreme precipitation caused by Atlantic variability and climate change. *Wea. Climate Extremes*, **33**, 100351, https://doi.org/10.1016/j.wace.2021.100351.

Ivancic, T. J., and S. B. Shaw, 2016: A U.S.-based analysis of the ability of the Clausius-Clapeyron relationship to explain changes in extreme rainfall with changing temperature. *J. Geophys. Res. Atmos.*, **121**, 3066–3078, https://doi.org/10.1002/2015JD024288.

Kao, S.-C., and A. R. Ganguly, 2011: Intensity, duration, and frequency of precipitation extremes under 21st-century warming scenarios. *J. Geophys. Res.*, **116**, D16119, https://doi.org/10.1029/2010JD015529.

Karmalkar, A. V., 2018: Interpreting results from the NARCCAP and NA-CORDEX ensembles in the context of uncertainty in regional climate change projections. *Bull. Amer. Meteor. Soc.*, **99**, 2093–2106, https://doi.org/10.1175/BAMS-D-17-0127.1.

——, and R. M. Horton, 2021: Drivers of exceptional coastal warming in the northeastern United States. *Nat. Climate Change*, **11**, 854–860, https://doi.org/10.1038/s41558-021-01159-7.

Kharin, V. V., F. W. Zwiers, X. Zhang, and M. Wehner, 2013: Changes in temperature and precipitation extremes in the CMIP5 ensemble. *Climatic Change*, **119**, 345–357, https://doi.org/10.1007/s10584-013-0705-8.

Kirchmeier-Young, M. C., F. W. Zwiers, N. P. Gillett, and A. J. Cannon, 2017: Attributing extreme fire risk in western Canada to human emissions. *Climatic Change*, **144**, 365–379, https://doi.org/10.1007/s10584-017-2030-0.

Kirschbaum, D., R. Adler, D. Adler, C. Peters-Lidard, and G. Huffman, 2012: Global distribution of extreme precipitation and high-impact landslides in 2010 relative to previous years. *J. Hydrometeor.*, **13**, 1536–1551, https://doi.org/10.1175/JHM-D-12-02.1.

Knist, S., and Coauthors, 2017: Land-atmosphere coupling in EURO-CORDEX evaluation experiments. *J. Geophys. Res. Atmos.*, **122**, 79–103, https://doi.org/10.1002/2016JD025476.

Kocin, P. J., and L. W. Uccellini, 2004: *Northeast Snowstorms.* Vols. 1 and 2, *Meteor. Monogr.*, No. 54, Amer. Meteor. Soc., 818 pp.

Kunkel, K. E., and Coauthors, 2013: Monitoring and understanding trends in extreme storms: State of knowledge. *Bull. Amer. Meteor. Soc.*, **94**, 499–514, https://doi.org/10.1175/BAMS-D-11-00262.1.

Langhans, W., K. Yeo, and D. M. Romps, 2015: Lagrangian investigation of the precipitation efficiency of convective clouds. *J. Atmos. Sci.*, **72**, 1045–1062, https://doi.org/10.1175/JAS-D-14-0159.1.

Leung, L. R., L. O. Mearns, F. Giorgi, and R. L. Wilby, 2003: Regional climate research: Needs and opportunities. *Bull. Amer. Meteor. Soc.*, **84**, 89–95, https://doi.org/10.1175/BAMS-84-1-89.

Lopez-Cantu, T., A. F. Prein, and C. Samaras, 2020: Uncertainties in future U.S. extreme precipitation from downscaled climate projections. *Geophys. Res. Lett.*, **47**, e2019GL086797, https://doi.org/10.1029/2019GL086797.

Lucas-Picher, P., R. Laprise, and K. Winger, 2017: Evidence of added value in North American regional climate model

hindcast simulations using ever-increasing horizontal resolutions. *Climate Dyn.*, **48**, 2611–2633, https://doi.org/10.1007/s00382-016-3227-z.

Lutsko, N. J., and T. W. Cronin, 2018: Increase in precipitation efficiency with surface warming in radiative-convective equilibrium. *J. Adv. Model. Earth Syst.*, **10**, 2992–3010, https://doi.org/10.1029/2018MS001482.

Martinez-Villalobos, C., and J. D. Neelin, 2019: Why do precipitation intensities tend to follow gamma distributions? *J. Atmos. Sci.*, **76**, 3611–3631, https://doi.org/10.1175/JAS-D-18-0343.1.

McGinnis, S., and L. Mearns, 2021: Building a climate service for North America based on the NA-CORDEX data archive. *Climate Serv.*, **22**, 100233, https://doi.org/10.1016/j.cliser.2021.100233.

Muller, C., and Y. Takayabu, 2020: Response of precipitation extremes to warming: What have we learned from theory and idealized cloud-resolving simulations, and what remains to be learned? *Environ. Res. Lett.*, **15**, 035001, https://doi.org/10.1088/1748-9326/ab7130.

Myhre, G., and Coauthors, 2019: Frequency of extreme precipitation increases extensively with event rareness under global warming. *Sci. Rep.*, **9**, 16063, https://doi.org/10.1038/s41598-019-52277-4.

Nazarian, R., 2021: The use of model intercomparison projects in engaging undergraduates in climate change research. *Scholarship Pract. Undergrad. Res.*, **5**, 27–28, https://doi.org/10.18833/spur/5/1/8.

Ning, L., E. E. Riddle, and R. S. Bradley, 2015: Projected changes in climate extremes over the northeastern United States. *J. Climate*, **28**, 3289–3310, https://doi.org/10.1175/JCLI-D-14-00150.1.

Nishant, N., and S. C. Sherwood, 2021: How strongly are mean and extreme precipitation coupled? *Geophys. Res. Lett.*, **48**, e2020GL092075, https://doi.org/10.1029/2020GL092075.

O'Gorman, P. A., 2014: Contrasting responses of mean and extreme snowfall to climate change. *Nature*, **512**, 416–418, https://doi.org/10.1038/nature13625.

——, 2015: Precipitation extremes under climate change. *Curr. Climate Change Rep.*, **1**, 49–59, https://doi.org/10.1007/s40641-015-0009-3.

Pendergrass, A. G., and E. P. Gerber, 2016: The rain is askew: Two idealized models relating vertical velocity and precipitation distributions in a warming world. *J. Climate*, **29**, 6445–6462, https://doi.org/10.1175/JCLI-D-16-0097.1.

——, F. Lehner, B. M. Sanderson, and Y. Xu, 2015: Does extreme precipitation intensity depend on the emission scenario? *Geophys. Res. Lett.*, **42**, 8767–8774, https://doi.org/10.1002/2015GL065854.

——, K. A. Reed, and B. Medeiros, 2016: The link between extreme precipitation and convective organization in a warming climate: Global radiative-convective equilibrium simulations. *Geophys. Res. Lett.*, **43**, 11 445–11 452, https://doi.org/10.1002/2016GL071285.

Pithan, F., and T. Mauritsen, 2014: Arctic amplification dominated by temperature feedbacks in contemporary climate models. *Nat. Geosci.*, **7**, 181–184, https://doi.org/10.1038/ngeo2071.

Rastogi, D., D. Touma, K. J. Evans, and M. Ashfaq, 2020: Shift toward intense and widespread precipitation events over the United States by mid-21st century. *Geophys. Res. Lett.*, **47**, e2020GL089899, https://doi.org/10.1029/2020GL089899.

Rawlins, M. A., R. S. Bradley, and H. F. Diaz, 2012: Assessment of regional climate model simulation estimates over the northeast United States. *J. Geophys. Res.*, **117**, D23112, https://doi.org/10.1029/2012JD018137.

Rendfrey, T., M. Bukovsky, R. McCrary, and R. Fuentes-Franco, 2021: An assessment of tropical cyclones in North American CORDEX WRF simulations. *Wea. Climate Extremes*, **34**, 100382, https://doi.org/10.1016/j.wace.2021.100382.

Rosenzweig, C., F. N. Tubiello, R. Goldberg, E. Mills, and J. Bloomfield, 2002: Increased crop damage in the US from excess precipitation under climate change. *Global Environ. Change*, **12**, 197–202, https://doi.org/10.1016/S0959-3780(02)00008-0.

Schär, C., and Coauthors, 2016: Percentile indices for assessing changes in heavy precipitation events. *Climatic Change*, **137**, 201–216, https://doi.org/10.1007/s10584-016-1669-2.

Schwalm, C. R., S. Glendon, and P. B. Duffy, 2020: RCP8.5 tracks cumulative CO_2 emissions. *Proc. Natl. Acad. Sci. USA*, **117**, 19 656–19 657, https://doi.org/10.1073/pnas.2007117117.

Sheffield, J., and Coauthors, 2013: North American climate in CMIP5 experiments. Part I: Evaluation of historical simulations of continental and regional climatology. *J. Climate*, **26**, 9209–9245, https://doi.org/10.1175/JCLI-D-12-00592.1.

Sillmann, J., V. V. Kharin, F. W. Zwiers, X. Zhang, and D. Bronaugh, 2013: Climate extremes indices in the CMIP5 multimodel ensemble: Part 2. Future climate projections. *J. Geophys. Res. Atmos.*, **118**, 2473–2493, https://doi.org/10.1002/jgrd.50188.

Singh, J., S. Karmakar, D. PaiMazumder, S. Ghosh, and D. Niyogi, 2020: Urbanization alters rainfall extremes over the contiguous United States. *Environ. Res. Lett.*, **15**, 074033, https://doi.org/10.1088/1748-9326/ab8980.

Singh, M. S., and P. A. O'Gorman, 2014: Influence of microphysics on the scaling of precipitation extremes with temperature. *Geophys. Res. Lett.*, **41**, 6037–6044, https://doi.org/10.1002/2014GL061222.

Soares, P. M. M., J. A. M. Careto, R. M. Cardoso, K. Goergen, and R. M. Trigo, 2019: Land-atmosphere coupling regimes in a future climate in Africa: From model evaluation to projections based on CORDEX-Africa. *J. Geophys. Res. Atmos.*, **124**, 11 118–11 142, https://doi.org/10.1029/2018JD029473.

Steinschneider, S., and N. Najibi, 2022: Observed and projected scaling of daily extreme precipitation with dew point temperature at annual and seasonal scales across the northeast United States. *J. Hydrometeor.*, **23**, 403–419, https://doi.org/10.1175/JHM-D-21-0183.1.

Tabari, H., 2020: Climate change impact on flood and extreme precipitation increases with water availability. *Sci. Rep.*, **10**, 13768, https://doi.org/10.1038/s41598-020-70816-2.

Tamarin-Brodsky, T., and O. Hadas, 2019: The asymmetry of vertical velocity in current and future climate. *Geophys. Res. Lett.*, **46**, 374–382, https://doi.org/10.1029/2018GL080363.

Thibeault, J. M., and A. Seth, 2014: Changing climate extremes in the northeast United States: Observations and projections from CMIP5. *Climatic Change*, **127**, 273–287, https://doi.org/10.1007/s10584-014-1257-2.

Walsh, J., and Coauthors, 2014: Our changing climate. *Climate Change Impacts in the United States: The Third National Climate Assessment*, J. M. Melillo, T. Richmond, and G. W. Yohe, Eds., U.S. Global Change Research Program, 19–67.

Wang, G., C. J. Kirchhoff, A. Seth, J. T. Abatzoglou, B. Livneh, D. W. Pierce, L. Fomenko, and T. Ding, 2020: Projected changes of precipitation characteristics depend on downscaling method and training data: MACA versus LOCA using

the U.S. northeast as an example. *J. Hydrometeor.*, **21**, 2739–2758, https://doi.org/10.1175/JHM-D-19-0275.1.

Wilhelmi, O. V., and R. E. Morss, 2013: Integrated analysis of societal vulnerability in an extreme precipitation event: A Fort Collins case study. *Environ. Sci. Policy*, **26**, 49–62, https://doi.org/10.1016/j.envsci.2012.07.005.

Zarzycki, C. M., 2018: Projecting changes in societally impactful northeastern U.S. snowstorms. *Geophys. Res. Lett.*, **45**, 12 067–12 075, https://doi.org/10.1029/2018GL079820.

Zscheischler, J., and Coauthors, 2018: Future climate risk from compound events. *Nat. Climate Change*, **8**, 469–477, https://doi.org/10.1038/s41558-018-0156-3.